IEEE Access
Multidisciplinary | Rapid Review | Open Access Journal

Received November 14, 2019, accepted December 2, 2019, date of publication December 13, 2019,
date of current version December 23, 2019.

Digital Object Identifier 10.1109/ACCESS.2019.2958940

A Co-Simulation Method Based on Coupled Thermoelectric Model for Electrical and Thermal Behavior of the Lithium-ion Battery

WEINAN HUANG[1], WEIGE ZHANG[1], ANCI CHEN[1], YANRU ZHANG[1], AND MING LI[2]
[1]National Active Distribution Network Technology Research Center (NANTEC), Beijing Jiaotong University, Beijing 100044, China
[2]CRRC Tangshan Company, Ltd., Tangshan 064000, China

Corresponding author: Yanru Zhang (yr_zhang@bjtu.edu.cn)

This work was supported by the National Key Research and Development Program of China under Grant 2017YFB1201003.

ABSTRACT Nowadays, the lithium-ion battery (LIB) has been widely used as an energy source for electric vehicles or the auxiliary power supply for rail transit. However, the sensitivity of LIB to temperature greatly limits its application condition. Due to internal impedance and entropy change, temperature of LIB varies during charging and discharging. This variation conversely affects the electrical characteristics of batteries, and then the heat generation rate. In order to accurately model this coupled thermoelectric process of the lithium-ion battery, a co-simulation method based on coupled thermoelectric model is developed in this paper, which combines equivalent circuit model (ECM) and Computational Fluid Dynamics (CFD) software. For purpose of verifying the feasibility and accuracy of the proposed method, Experiments are performed at different temperatures and C-rates conditions, using a large-format pouch cell applied in rail transit projects. The comparison indicates that this method joined with temperature correction has higher accuracy than the traditional thermal simulation without temperature correction and the simulated result shows good agreement with measurements.

INDEX TERMS Lithium-ion battery, coupled thermoelectric model, co-simulation method.

I. INTRODUCTION

Lithium-ion batteries have been widely used in electric vehicles and rail transit industry due to their high-power density, low self-discharge rate and environmental friendliness [1]–[4]. Therefore, the safety of lithium-ion batteries has attracted wide attention from researchers. Temperature plays an important role of safety when using batteries: if the temperature is too low, not only the available capacity of the battery will be greatly reduced, but the output power as well [5], [6]. Long-term usage at low temperature will lead to internal lithium deposition and lithium dendrite, which poses a safety hazard; While high temperature can incur the decomposition of the battery electrolyte and thus induce thermal runaway [7]–[9], causing a fire accident. Thence battery thermal management system (BTMS) is an important guarantee for ensuring thermal safety.

The associate editor coordinating the review of this manuscript and approving it for publication was Fei Lu.

Thermal simulation plays an important role in the design of BTMS [10]. Accurate simulation results can predict its control effect on the battery temperature, providing reference for optimizing BTMS. By using simulation, BTMS is checked to meet the actual needs. Avoiding repeated verification by using physical objects and reducing system development costs, this process can greatly reduce the workload of the previous design and save development costs.

In the field of thermal simulation, Kim *et al.* [11] and Xiao *et al.* [12] analyzed the battery heat generation process from the electrochemical perspective, but the parameters involved were numerous and can be hardly measured, causing the difficulty of using electrochemical-thermal coupling model for practical application; Comparatively ECM-based thermal simulation is easier to realize and widely used, because ECM parameters, which are easy to measure, highly summarize the electrochemical reaction process of batteries. In addition, the accuracy is proved [13], [14].

The thermal changes caused by electrical factors will in turn affect the electrical characteristics of the battery.

Therefore, the heat generation of the battery is a process in which complex thermoelectric coupling exists. Wang *et al.* [15] used finite element method to numerically simulate a cylindrical lithium-ion battery and analyzed battery core temperature by changing convection cooling conditions. Jaguemont *et al.* [16] simulated the change of equivalent parameters of battery at normal and low temperature. Duan *et al.* [17] used the simplified Bernardi equation to perform a thermal simulation analysis of the battery module. They did not show the effect of temperature on electrical parameters, that is, an incomplete thermoelectric coupling process. In addition the irreversible heat of the battery was reduced to the product of the square of the current and the internal resistance, the influence of the capacitive effect was neglected, leading to remarkable error; Kim *et al.* [18], [19] used a two-dimensional (the thickness direction is ignored) model to simulate the voltage distribution of discharge process of a stacked lithium-ion battery, and calculated the two-dimensional temperature field distribution of the single cell based on the voltage distribution. The terminal voltage simulation results are accurate, but the temperature simulation results existed big errors. The reason is that the heat generation curves at different temperatures derived according to the Arrhenius formula and the Nernst equation, were not corrected according to the real-time temperature. What's more, the model is not verified by the charging process; Chen *et al.* [20] established a three-dimensional distributed battery model based on finite element, implanting the first-order RC circuit model and a heat transfer model into each volume micro-element to realize the thermoelectric coupling process. They obtained the current, density distribution and temperature field of the single cell; Chen *et al.* [21] adopted a similar distributed model and selected several locations of single cells for temperature monitoring to prove the accuracy of the simulation. However, the simulation calculation is more complicated and not suitable for simulation at the battery module or pack.

In this paper, a thermoelectric co-simulation method is developed, which combines ECM and CFD simulation. ECM is established in OpenModelica environment, a software that is often used in vehicle system simulation, with the advantages of equation programming and fast solution of differential equations. Besides, ECM based on Modelica language has the function of connecting with other graphical electrical components, which provides the possibility for the thermal simulation of the whole vehicle system in existing simulation platforms, such as MATLAB. The influence of the state of charge (SOC), temperature, current direction, and C-rate on ECM parameters is taken into consideration to change parameters according to the battery's own state during charging and discharging process. The battery terminal voltage and heat generation rate calculated in OpenModelica environment are entered into ANSYS Fluent, a widely used commercial CFD software. Whereafter, the battery temperature field is simulated according to the boundary conditions and the physical structure. Subsequently the average volume temperature of the battery is re-entered into ECM, and the coupling between the zero-dimensional electrical model and the three-dimensional heat transfer model is realized. Since the equivalent circuit simulation calculates fast, and CFD simulation takes a long time, the timing of both needs to be arbitrated by a third party. Therefore, interface script based on Python language is developed.

The paper is structured as follows. Firstly, the basic principle of the thermoelectric coupling model and its implementation process in the co-simulation method are introduced in Section II. In Section III, the methods for identifying the ECM parameters and measuring thermal properties of battery are expounded. Finally, the effectiveness of this method is verified by analyzing deviations between the results of simulation and experiment in Section IV, with a large-format lithium titanate pouch cell as the target.

II. THE PRINCIPLE OF THE THERMOELECTRIC COUPLING MODEL AND CO-SIMULATION METHOD

A. THE THERMOELECTRIC COUPLING MODEL

Bernardi *et al.* [22] rationally simplified the heat generation mechanism of battery, obtained a simplified equation. They ignored the uneven heat generation and phase change heat generation of the battery reactants, only retained the irreversible heat generated by the internal resistance of the battery and the reversible heat originated from the entropy change, which made the equation simpler and the parameters were easy to measure. The battery heat generation model is as shown in (1):

$$q = I(U - E_{OC}) + IT\frac{\partial E_{OC}}{\partial T} \tag{1}$$

where q is the unit heat generation power per unit cell, I is the battery current (assumed to be positive in charge period), E_{OC} is the open circuit voltage (OCV), U is the terminal voltage, and T is the temperature. It can be seen from the Bernardi equation that the irreversible heat term $I(U - E_{OC})$ describes the heating power caused by the difference between the battery terminal voltage and OCV. The reversible heat term $IT(\partial E_{OC}/\partial T)$ depends on the battery temperature, the battery current and the entropy coefficient (inherent constant). Thus, the basis of an accurate heat generation model is the precise terminal voltage model.

In this paper, the simplified Bernardi equation is adopted to analyze the heat power of battery. When calculating the irreversible heat term, the terminal voltage and OCV of battery existing in Bernardi equation need to be obtained according to battery ECM. There are many types of battery ECMs [23]–[25], such as Thevenin model (first-order RC circuit model) and second-order RC model. Thevenin model, which is chosen in this article, has characteristics of simple

structure (a single RC parallel network in series with a resistance), few parameters, easy parameter identification [26], and high accuracy for the description of battery terminal voltage. The equivalent circuit topology diagram and mathematical terminal voltage formula are shown in Figure 1 and

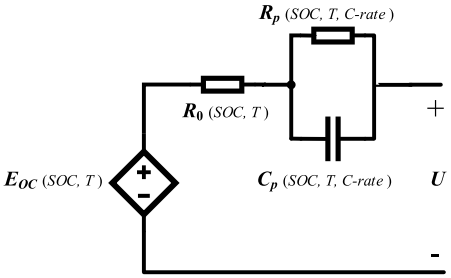

FIGURE 1. Thevenin model of lithium-ion battery.

(2) respectively.

$$U = E_{OC} + IR_0 + IR_p[1 - \exp(-\frac{t}{R_pC_p})] \tag{2}$$

where R_0, the ohmic internal resistance, characterizes the equivalent internal resistance of the instantaneous change of terminal voltage when battery is excited by the mutated current. R_0 originates from the potential difference generated when current flows through separators, current collector and the positive and negative pole pieces [27]. R_p and C_p characterize the process in which battery undergoes a slow change in the voltage at the back end of current excitation, that is, the polarization impedance. The practical significance is to describe charge transfer, diffusion and the time lag of lithium ions derived from the difference in concentration.

It is noticed that substituting the terminal voltage expression into (1) can obtain the heat power of battery. After analyzing the heat transfer result of battery, the parameters affected by temperature in circuit model are corrected according to the feedback temperature, and the thermoelectric coupling model can be established, as shown in the Figure 2.

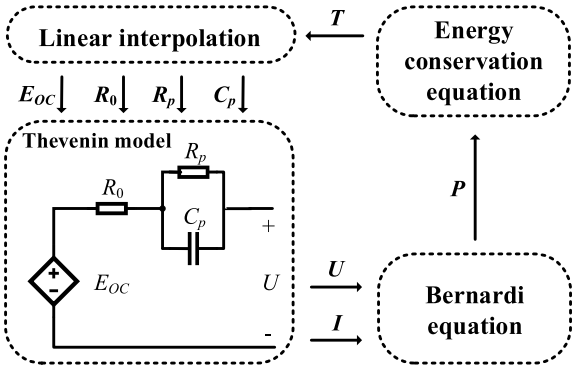

FIGURE 2. Thermoelectric coupling model of lithium-ion battery.

B. THE PRINCIPLE OF BATTERY HEAT TRANSFER

From the circuit model we can only get the heat power generated by battery. To get the battery temperature, we need to analyze it from the perspective of heat transfer. CFD simulation software can quantitatively describe the temperature field distribution of an object by numerical calculation. The temperature distribution of battery can be computed after the heat power is input into the model of CFD software, with calculation solved according to boundary conditions. The three-dimensional heat transfer equation is:

$$\rho C\frac{\partial T}{\partial t} = \nabla \cdot (k\nabla T) + q - q_{diss} \tag{3}$$

where ρ is the density, C is the specific heat capacity, k is the thermal conductivity, q is the heat generation rate per unit volume, and q_{diss} is the heat dissipation rate per unit volume to the outside. It can be calculated from (4) when only the heat convection is taken into account:

$$q_{diss} = hA(T - T_A) \tag{4}$$

where h is the convection heat transfer coefficient of the battery surface, A is the surface area of battery, T_A is the environmental temperature.

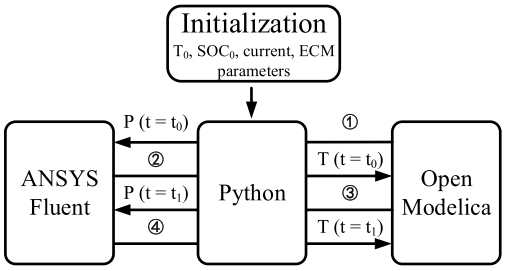

FIGURE 3. Co-simulation procedure.

C. THERMAL CO-SIMULATION FRAMEWORK FOR TEMPERATURE CORRECTION

The thermal co-simulation framework is shown in Figure 3. The circuit and CFD simulation software are OpenModelica and Ansys Fluent, respectively, of which the simulation process and data exchange are controlled by Python code. At the beginning of simulation, the circuit model needs to be initialized on the basis of initial temperature T0, initial state of charge SOC0, RC parameters, charge and discharge current, cutoff conditions, and simulation step size.

OpenModelica simulates the battery terminal voltage and real-time heat power P ($t = t_0$) according to (1) and (2), which will be sent to specified storage space of Python. Python code suspends the simulation process of OpenModelica and sends the obtained data to the CFD software. Then CFD software simulates the temperature field of battery and outputs the average volume temperature, T ($t = t_0$), of battery, according to which the circuit model parameters are updated. After that OpenModelica calculates a new heat power P ($t = t_1$) based on changed parameters which will be used for next calculation to simulate the thermoelectric coupling process with temperature correction.

III. EXPERIMENTAL SETUP AND PROCEDURES

The experimental platform is shown in Figure 5. The battery test equipment used in experiment is Maccor Series 4000, and temperature recording equipment is the wireless

TABLE 1. Basic parameters of battery.

Parameter name	Specification
Battery type	Lithium titanate
Nominal voltage	2.35V
Charge/Discharge cutoff voltage	2.8/1.5V
Mass	0.70±0.03kg
Nominal capacity (25℃, 100%DOD, 1C)	25Ah

data acquisition device LR8410-30 with the measuring unit LR8511 produced by Hioki (Shanghai) Trading Company, Ltd. All the measurements, such as voltage, current, temperature, are collected per second. In this paper, a commercial large-format lithium titanate stacked pouch cell is chosen as the research object, whose ears are located on both short sides of the rectangular body. The specific parameters are shown in Table 1.

In the ECM parameters identification experiment, the cell is placed in a thermal chamber, whose temperature is set to 25°C, and fully rests until the cell temperature is stable to ambient temperature. Subsequently, it is charged to 100% SOC by constant current and constant voltage (CCCV) method. The current rate of constant process is 1C (25A), and the cutoff condition is 0.05C (1.25A). The reason for choosing this identification method will be explained later. After fully resting, SOC is adjusted to 91% by 1C current, and then a Hybrid Pulse Power Characterization (HPPC) is applied to the cell. First, the cell is discharged to 90% SOC with 1C. The data during depolarization is used for ECM parameters identification. After resting for 10 min, SOC is corrected to 89% with 0.1C current. The cell is afterwards charged to 90%SOC with the same rate, and the current is changed to 2C (50A), 3C (75A), and 4C (100A) for other pulse test respectively. After that, V-I curves are measured in the same way at different SOC points (90%∼10%, interval 5%) and different temperatures (5°C, 15°C, 25°C, 45°C). The first 15s pulse test data is fitted by the least squares method to identify the ECM parameters R_0, R_p, C_p. Finally, OCV is measured after the cell fully rests at different temperature points (5°C, 15°C, 25°C, 45°C) and different SOC points (0%∼100%, interval 5%).

In order to verify the accuracy of this method, four sets of comparative tests are carried out. Charge and discharge experiments are performed at different temperatures and C-rates, simulations carried out correspondingly. The accuracy of simulation is determined by analyzing the error of terminal voltage curve and temperature change curve. The center points of extension surfaces on both sides of the battery are selected as temperature measured points, the arithmetic means of whose values at the same moment are deemed as battery temperature values. The battery temperature is firstly adjusted to 25°C, with SOC set to 90% by ampere-hour integral, and then the cell is discharged to 10% SOC with 1C, 1.5C, 2C, 2.5C, 3C, 3.5C and 4C respectively. After that, the opposite process is performed.

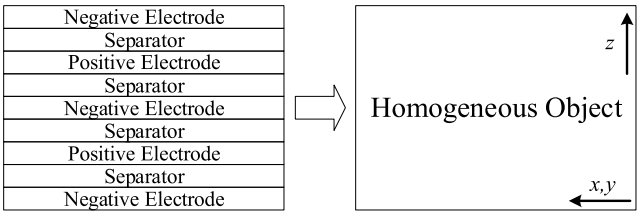

FIGURE 4. Schematic diagram of a layered structure simplified to a homogeneous object.

In the temperature verification experiment, the battery rests in the chamber at 20°C, 30°C, 40°C respectively, and then 4C charge and discharge experiments are performed.

A. PARAMETER IDENTIFICATION

To simplify the battery model, the following assumptions are made:

1) In the circuit model, the spatial distribution of electrochemical reaction process of cell is considered to be approximately uniform, the difference in internal concentration, phase transition, and potential of monomer ignored.
2) The thermophysical parameters of cell do not change as the electrochemical reaction proceeds.
3) The internal of the cell is superposed by pole pieces, separators, etc., and the thickness of each layer is extremely thin. Therefore, the difference of thermal property parameters between layers can be neglected, and the internal laminated structure of the cell is simplified into a uniform whole [28]. As shown in Figure 4, the distribution of materials is uniform, and the inherent values of the overall density, specific heat capacity, and thermal conductivity (every direction) of the cell can be described by an identical equivalent value.
4) The interior of the cell is equivalent to a uniform heating element, and the same heat power is given to each volume unit of cell body during the simulation.
5) The cell has different thermal conductivity in three dimensions. Due to the structural characteristics of stacked pole pieces and separators, the thermal resistance is connected in series in z direction, and in parallel in x and y direction (with the same value). Thus, only two thermal conductivity values are needed to describe the heat transfer process in three dimensions.
6) The influence of package such as aluminum plastic film on the outer surface of cell is neglected, and the cell is simplified into a combination of internal material and tabs, the connections among which are represented by small air gaps [29].

B. CIRCUIT PARAMETER IDENTIFICATION

In order to prevent SOC from shifting when the HPPC pulse is applied, the battery SOC is first adjusted to a point slightly higher (or lower) than the target value, and then discharged (charged) to the target SOC value by pulse.

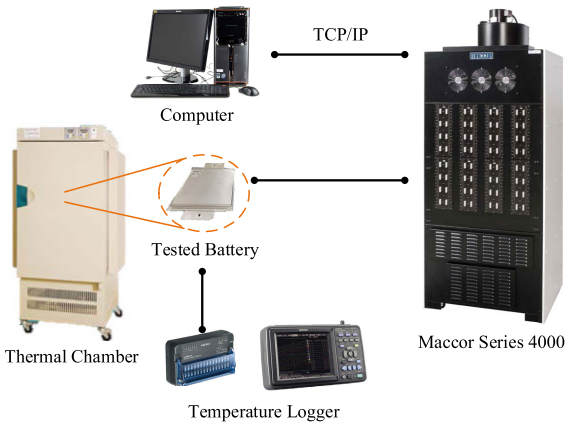

FIGURE 5. Experiment platform.

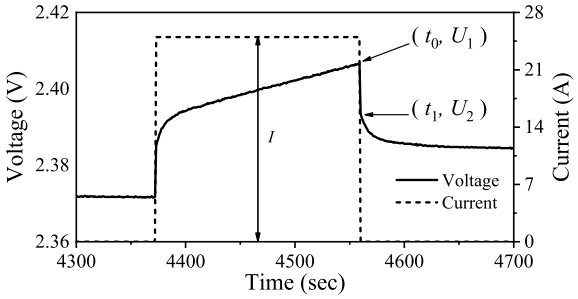

FIGURE 6. RC parameter identification curve.

According to Thevenin model, the voltage versus time curve can be obtained by applying abrupt current to battery, and the parameters in the model can be identified according to the curve, as shown in Figure 6. It is known from the physical meaning that R_0 is equal to the voltage change of battery at the moment of excitation divided by the current at the previous moment:

$$R_0 = \frac{U_1 - U_2}{I} = \frac{\Delta V_0}{I} \tag{5}$$

where U_1 is the voltage value at the moment when the current is suddenly changed. Since the terminal voltage curve is not a total terminal voltage response of the first-order RC circuit, the actual response should be an oblique line with a certain slope, not a step response curve. Therefore, U_2 is taken as the voltage value at the next discretization sampling time after the sudden change of current, and I is taken as the battery current at the moment before sudden change. The polarization internal resistance R_p, C_p can be obtained by performing the least square fit on the voltage data during the depolarization process according to (2).

The parameter identification results is shown in Figure 7. As aforementioned, OCV change rate with temperature, the entropy coefficient, is shown in Figure 7(a) [28]. In order to prevent the temperature deviation of cell during the pulse test, finned radiators are added to the largest surfaces of cell body, and fans are used for forced convection heat dissipation in the experiment. The obtained ECM parameters are linearly interpolated in three dimensions of temperature, C-rate, and SOC. As mentioned above, all the ECM parameters required for simulation can be obtained. The identification results are shown in Figures 7(b) and (c). Ohmic resistance R_0 does not change with the vary of C-rate, which approximate exponentially decreases with the increase of temperature, but is not sensitive to the change of SOC [25]. In contrast, R_p and C_p are more susceptible to SOC than temperature.

C. THERMAL PROPERTY PARAMETER IDENTIFICATION

The density ρ of cell body except tabs can be calculated according to cell mass and tab volume provided by the manufacturer.

There are lots of ways to measure the specific heat capacity of cell. In literature [30], the specific heat capacity test approaches without special equipment are divided into cooling method and heating method according to temperature change. Although the experimental conditions required for these are relatively simple, large error exists. The Accelerating Rate Calorimeter (ARC) can effectively measure the specific heat capacity of battery [31]. Its procedure is: the cell is firstly placed in the ARC chamber, and the chamber temperature is tracked based on the value measured by thermocouple attached to cell. During the experiment, two batteries are used to clamp a lamellar heater with the same size as the surface of cell, which works at a known power P. Since the chamber can be assumed to be an adiabatic environment, the energy generated by heater is only used to heat the cell and raise its temperature without dissipation outside. Hereby, the specific heat capacity C is calculated according to the (6).

$$P = mC\frac{dT}{dt} \tag{6}$$

It is usually difficult to identify the convection heat transfer coefficient h of cell because even different parts of the same cell may have different heat transfer conditions. Therefore, the average convective heat transfer coefficient is introduced to describe the overall heat transfer process of the battery. The heat transfer coefficients of each part of cell are considered to be the same, with the process of thermal radiation being equivalent to convection heat transfer. Newton cooling law (7) can be written as (8), integral transformation performed.

$$mC\frac{dT}{dt} + hA(T - T_\infty) = 0 \tag{7}$$

$$T = T_\infty + (T_{\max} - T_\infty)e^{-\frac{hA}{mC}t} \tag{8}$$

where $T_{\max}$ is the cell temperature at the time t = 0. T_∞ is the cell temperature at which the cell eventually stabilizes. h, which is independent of the state of charge or discharge of cell and temperature, can be identified by fitting a cooling curve according to the (8). The temperature curve of discharging from 90% SOC to 10% SOC is selected as the fitting target data. (The greater temperature change, the smaller relative error of fitting).

The thermal conductivity of every direction can be calculated according to series-parallel formula. The cell can be

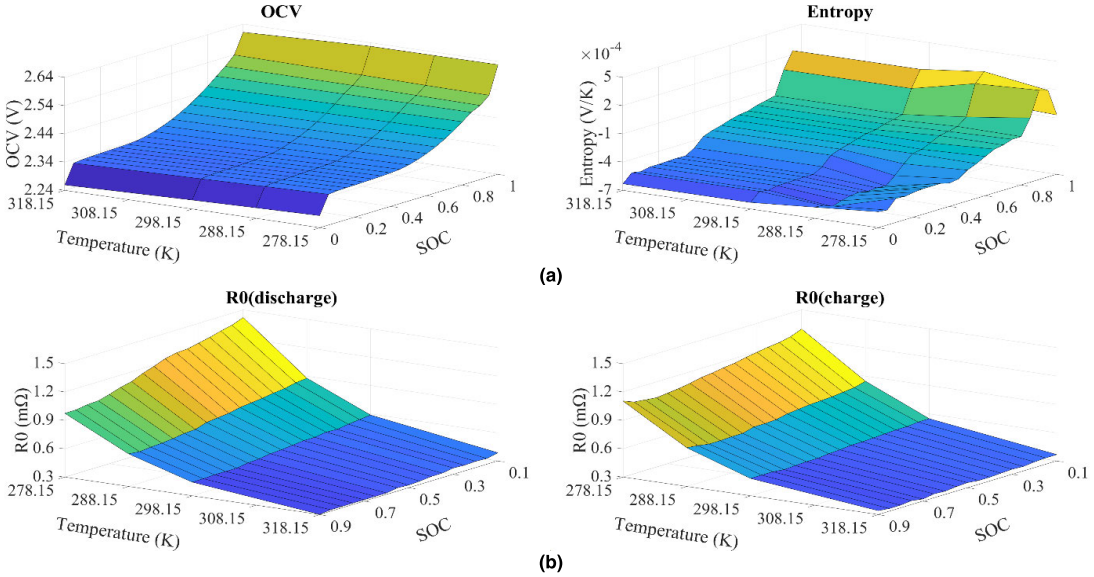

FIGURE 7. Circuit parameter identification result: (a) OCV and entropy coefficient; (b) R_0; (c) R_pC_p in the appendix.

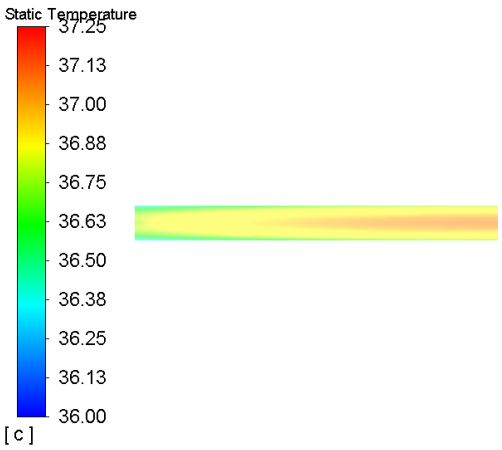

FIGURE 8. The contour of battery temperature of 4C discharge.

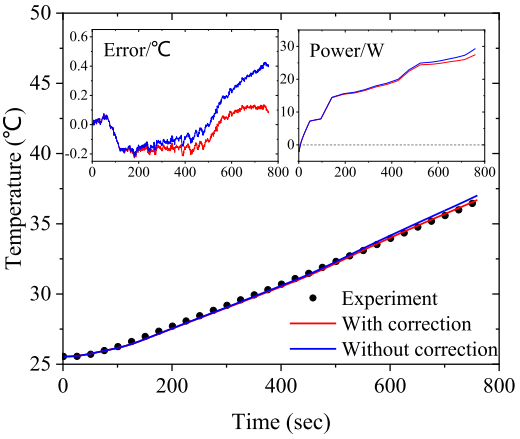

FIGURE 9. Comparison of whether there is temperature correction.

regarded as thermal resistance in series in thickness direction as (9), and in parallel in extension direction as (10). According to the internal material data provided by manufacturer, it can be calculated that thermal conductivity k_z of thickness direction equals about 30.79 W·m-1·K-1, and k_r of extension direction is approximately equal to 0.96 W·m-1·K-1. Thermal material properties of the battery materials are detailed in Table 2.

$$\frac{\sum_i d_i}{k_z} = \sum_i \frac{d_i}{k_i} \tag{9}$$

$$k_r \sum_i d_i = \sum_i k_i d_i \tag{10}$$

IV. EXPERIMENTAL VERIFICATION

The temperature contour along the length of the battery of 4C discharge is shown in Figure 8. Half of the contour image was shown because of its symmetry. Due to the thin body, the temperature difference of the battery in the thickness direction is not obvious, less than 1° after discharging for 760s with 4C. This phenomenon proves that for this battery, it is reasonable to select points on extension surfaces to measure temperature.

A. COMPARISON OF SIMULATION WITH AND WITHOUT TEMPERATURE CORRECTION

The conventional models usually do not have temperature correction. Figure 9 shows that simulation with temperature correction is more accurate than the one without. By comparison, it is found that the cell temperature change is not obvious at the beginning of process, with the similar results obtained by two simulations. However, as the process continues, the cell temperature changes greatly, and the error of simulation without temperature correction becomes larger and larger. The maximum error of correction-free simulation at the end is 0.32°C larger in temperature and 1.87W higher

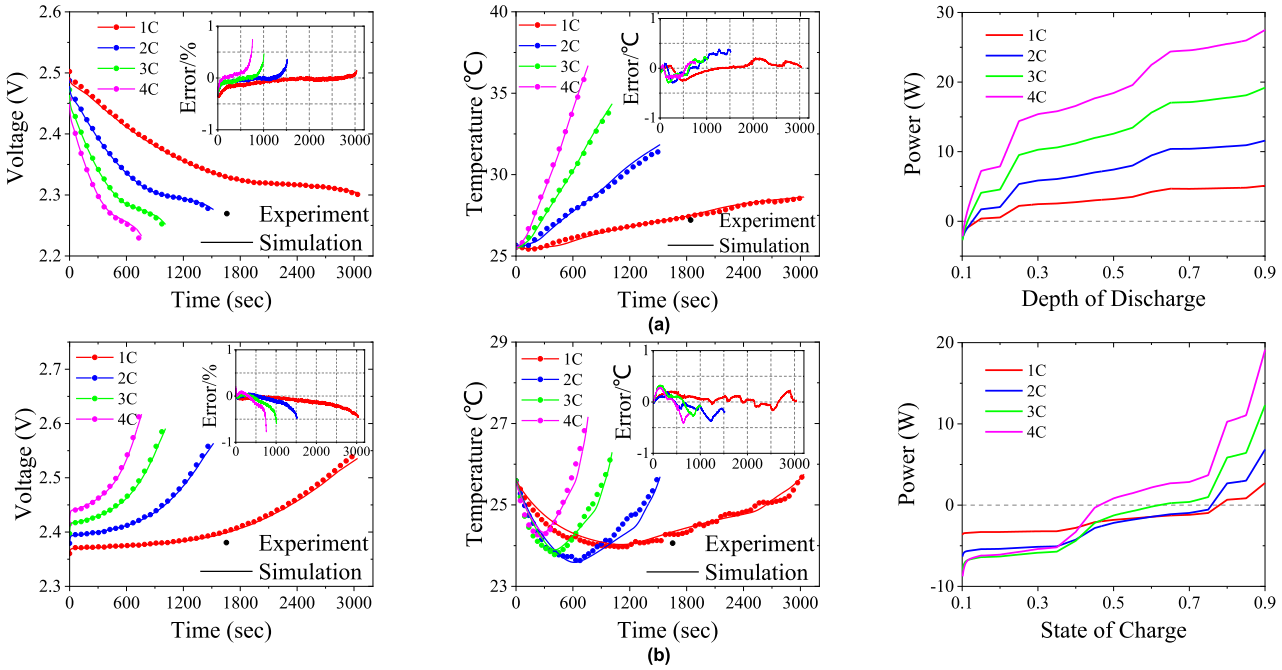

FIGURE 10. Comparison of experiment and simulation of 25°C at 1C to 4C: (a) discharge; (b) charge.

TABLE 2. Basic parameters of battery.

Parameter	Density /(kg·m-3)	Specific heat capacity /(J·kg-1·K-1)	Thermal conductivity /(W·m-1·K-1)	Thickness of each layer /(mm)
Positive electrode coating	2836	1173	1.85	0.067
Negative electrode coating (lithium titanate)	1667	1098	1.5	0.093
Separator	460	1978	0.334	0.025
Current collector (aluminum)	2702	903	238	0.015
Electrolyte	1187	2055	0.6	/
Aluminum plastic film	1456	1377	0.427	0.15

in power. As a power system consists of hundreds or even thousands of batteries, there will be huge cumulative deviations in estimating heat dissipation power for BTMS, causing in ill-designed system.

B. VERIFICATION OF C-RATES AT 25°C

The comparison results are shown in Figure 10. For the discharge process, it can be seen from voltage comparison that there are large errors in simulation results at the beginning and the end of discharging. The higher the C-rate, the larger the relative error is, reaching 0.74% at the end of 4C discharging. In the platform period, the accuracy is higher, with an error less than 0.3%. As shown in Figure 10 (a), temperature keeps rising in the discharge process, except for the initial stage (corresponding to high SOC). Combined with the simulated heat power curve and the variation of entropy coefficient, it can be seen that the battery is in an endothermic state during the discharge process firstly. Because of positive entropy coefficient and negative current value, the reversible heat power is negative. As the sum of negative reversible heat and positive irreversible heat, the total thermal power of cell is negative. Discharge process continuing, the entropy coefficient decreases rapidly, causing the total heat power changed from negative to positive.

Hereafter, under the dual action of entropy change and polarization, the heat power is further increased. When the heat power is higher than total dissipation power, the battery temperature begins to rise fast. The temperature error of discharging is kept within ±0.38°C.

Figure 10 (b) shows that, the simulated voltage is lower than the actual measurement for the charging process, except for the beginning phase. When SOC is higher than 50%, the relative error is more obvious, maximum reaching 0.77%. At the beginning of charging, the battery is

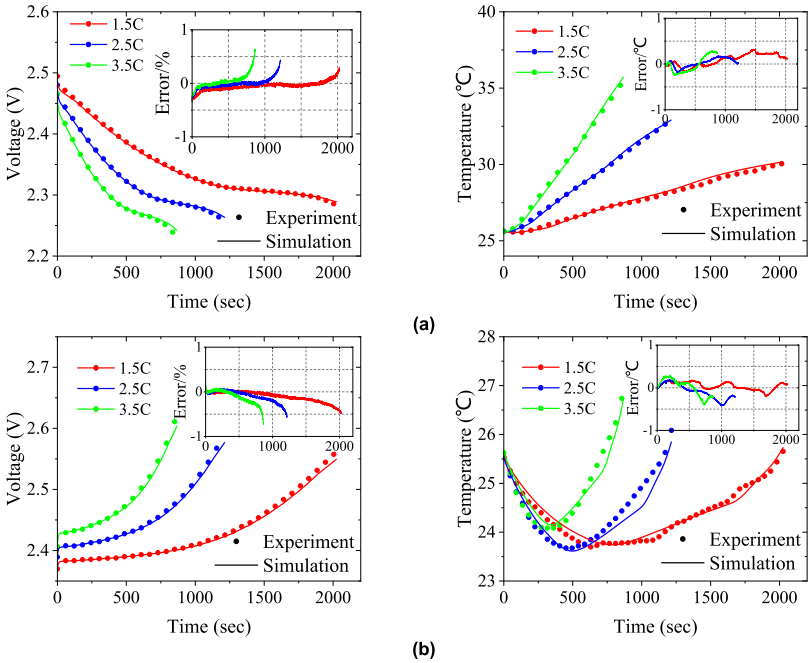

FIGURE 11. Comparison of experiment and simulation of 25°C at 1.5C to 3.5C: (a) discharge; (b) charge.

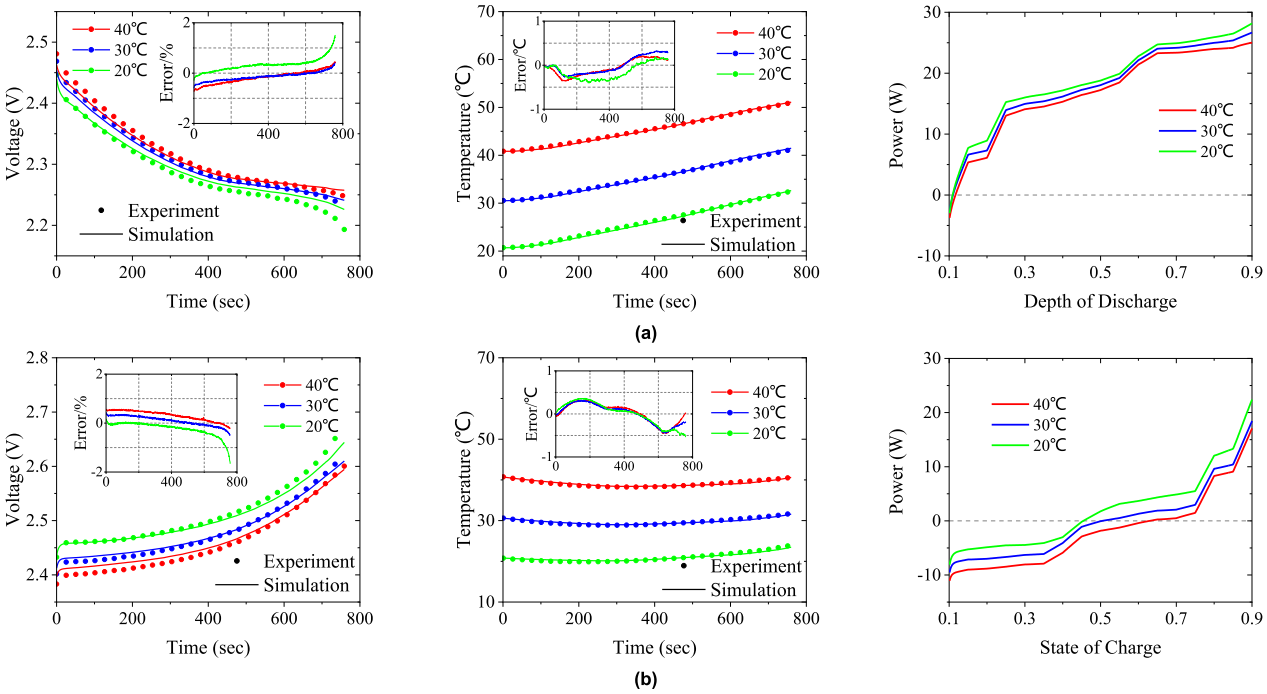

FIGURE 12. Comparison of experiment and simulation of 20°C to 40°C at 4C: (a) discharge; (b) charge.

endothermic, presenting a bowl-shaped temperature curve. As SOC reaches 43%, an inflection point occurs. According to the power curve, the battery generates a negative heat power at first, temperature dropping. The thermal difference between battery and environment cause heat transfer from environment to the cell, convection dissipation power keeping negative. When temperature drops to a certain critical value, the negative dissipation power is balanced with the heat generation power of battery. After that, the endothermic effect of entropy change weakens with the gradual increase of SOC. The reversible heat changes from endothermic to exothermic when SOC reaches 80%, leading to further raise of temperature. The maximum simulation error is approximately 0.41°C. In addition to the higher temperature at the

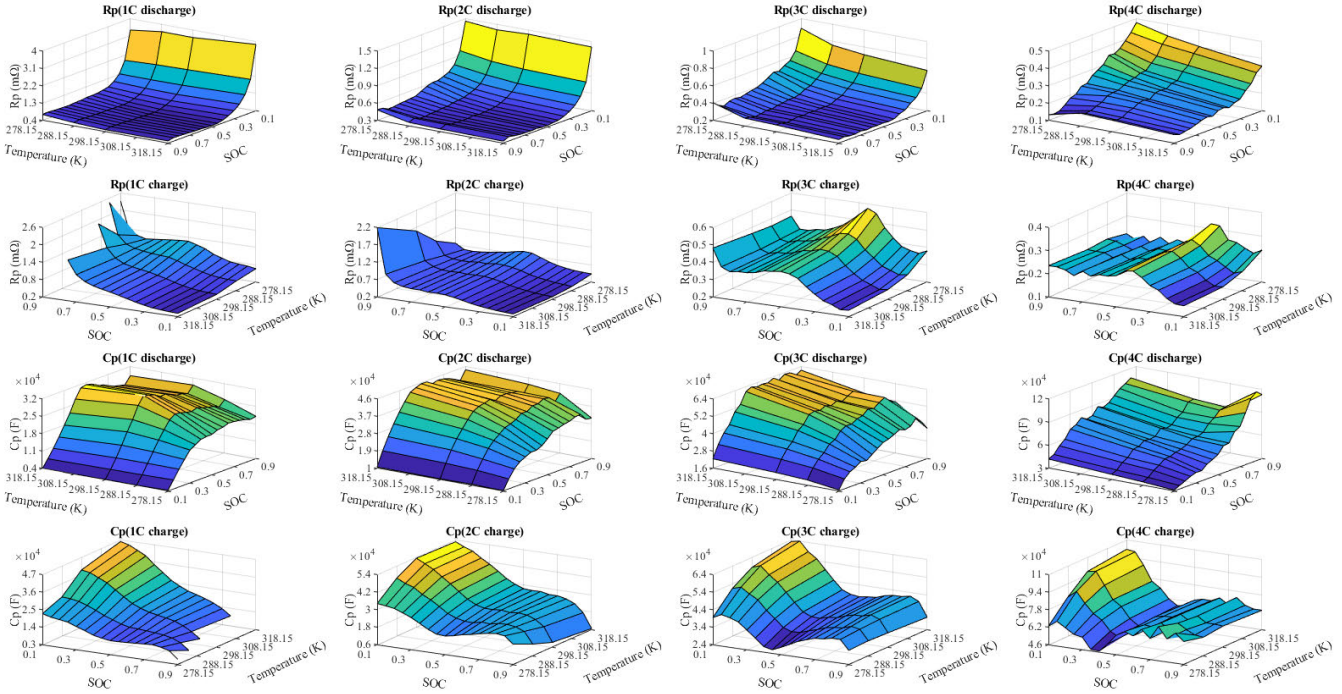

FIGURE 13. Circuit parameter identification result: (c) R_pC_p.

beginning, the values are lower than measurements. The reason is that: the initial simulated value of voltage is higher, bringing about a larger value of irreversible heat, ultimately a higher heat generation power; As charging process progresses, the simulated voltage is gradually lower than measurement, and the heat generation power is lower accordingly.

To further verify the accuracy, supplementary comparison of the same cell at 1.5C (37.5A), 2.5C (62.5A) and 3.5C (87.5A) is performed. Figure 11 shows the maximum errors of voltage and temperature occur at the end of 3.5C experiment, which are 0.64%, 0.29°C for discharging and 0.73%, and 0.40°C for charging respectively.

C. VERIFICATION OF TEMPERATURES AT 4C

The constant 4C charge and discharge experiments are performed at temperatures of 20°C, 30°C, 40°C. Figure 12(a) displays the larger errors occurring at the end of discharge, the peak value of which attains 1.50% at 20°C. The simulated voltage value at 20 °C is higher during the whole process. Since the polarization during discharging is opposite to charging, the simulated voltage drop of battery is smaller and the irreversible heat power is lower, reflected as lower simulation temperature. It can be seen from the voltage error curves that the simulation error is stable at 0.35% during the plateau period and the internal resistance of battery is about 0.075mΩ lower by calculation. Because the sharp increase of internal resistance at low temperatures, circuit parameters becomes inaccurate when there are few points for linear interpolation.

The voltage error for 30°C and 40°C is not obvious reversely. The errors at the beginning and the end are slightly larger, peaking at 0.74% for voltage and of 0.36°C for temperature. It can be seen from the power curve that the lower the temperature, the higher the heat generation power, which corresponds to the change of internal resistance with temperature. It also indicates that the battery itself has a certain adjustment ability for temperature: temperature decreases and heat generation power increases, causing temperature to change to an upward trend, and vice versa.

In Figure 12(b), with the larger initial value of simulated voltage and irreversible heat, battery temperature is higher. Afterwards, simulated voltage value becomes smaller, causing the temperature in a lower state.

V. CONCLUSION

In order to accurately describe the thermoelectric coupling process of battery, this paper establishes a thermal co-simulation method combining equivalent circuit simulation and CFD simulation. By comparing the simulation results with and without temperature correction, it is found that there is a large deviation in the calculation of heat generation power for correction-free results, which is not conducive to the well-designed BTMS; The accuracy and effectiveness of this method are verified by comparison of simulation and measurement at different temperatures and C-rates, which provides the possibility of thermal simulation of whole vehicle system, and a reliable pre-verification simulation tool for the design of battery system. The verification of the LIB module and package simulation is expected to be carried out in future work.

APPENDIX

See Figure 13.

REFERENCES

[1] B. Xu, A. Oudalov, A. Ulbig, G. Andersson, and D. S. Kirschen, "Modeling of lithium-ion battery degradation for cell life assessment," *IEEE Trans. Smart Grid*, vol. 9, no. 2, pp. 1131–1140, Mar. 2018.
[2] R. Xiong, Y. Zhang, H. He, X. Zhou, and M. Pecht, "A double-scale, particle-filtering, energy state prediction algorithm for lithium-ion batteries," *IEEE Trans. Ind. Electron.*, vol. 65, no. 2, pp. 1526–1538, Feb. 2018.
[3] M. A. Hannan, M. M. Hoque, A. Hussain, Y. Yusof, and P. J. Ker, "State-of-the-art and energy management system of lithium-ion batteries in electric vehicle applications: Issues and recommendations," *IEEE Access*, vol. 6, pp. 19362–19378, 2018.
[4] Z. Wang, J. Ma, and L. Zhang, "State-of-health estimation for lithium-ion batteries based on the multi-island genetic algorithm and the Gaussian process regression," *IEEE Access*, vol. 5, pp. 21286–21295, 2017.
[5] J. Jiang, H. Ruan, B. Sun, W. Zhang, W. Gao, L. Y. Wang, and L. Zhang, "A reduced low-temperature electro-thermal coupled model for lithium-ion batteries," *Appl. Energy*, vol. 177, pp. 804–816, Sep. 2016.
[6] J. Jiang, "A low-temperature internal heating strategy without lifetime reduction for large-size automotive lithium-ion battery pack," *Appl. Energy* vol. 230, pp. 257–266, Nov. 2018.
[7] F. Leng, C. M. Tan, M. Pecht, and J. Zhang, "The effect of temperature on the electrochemistry in Lithium-ion batteries," in *Proc. Int. Symp. Next-Gener. Electron. (ISNE)*, May 2014, pp. 1–4.
[8] S. Wilke, "Preventing thermal runaway propagation in lithium ion battery packs using a phase change composite material: An experimental study," *J. Power Sources*, vol. 340, pp. 51–59, Feb. 2017.
[9] I. Sho, K. Shah, and A. Jain, "Measurements and modeling to determine the critical temperature for preventing thermal runaway in Li-ion cells," *Appl. Therm. Eng.* vol. 145, pp. 287–294, Dec. 2018.
[10] L. H. Saw, A. A. O. Tay, and L. W. Zhang, "Thermal management of lithium-ion battery pack with liquid cooling," in *Proc. 31st Thermal Meas., Modeling Manage. Symp. (SEMI-THERM)*, Mar. 2015, pp. 298–302.
[11] G.-H. Kim, "Multi-domain modeling of lithium-ion batteries encompassing multi-physics in varied length scales," *J. Electrochem. Soc.*, vol. 158, no. 8, pp. A955–A969, 2011.
[12] M. Xiao and S.-Y. Choe, "Dynamic modeling and analysis of a pouch type LiMn2O4/Carbon high power Li-polymer battery based on electrochemical-thermal principles," *J. Power Sources*, vol. 218, pp. 357–367, Nov. 2017.
[13] G. Liu, L. Lu, J. Li, and M. Ouyang, "Thermal modeling of a $LiFePO_4$/graphite battery and research on the influence of battery temperature rise on EV driving range estimation," in *Proc. IEEE Vehicle Power Propuls. Conf. (VPPC)*, Oct. 2013, pp. 1–5.
[14] K. Murashko, J. Pyrhönen, and L. Laurila, "Three-dimensional thermal model of a lithium ion battery for hybrid mobile working machines: Determination of the model parameters in a pouch cell," *IEEE Trans. Energy Convers.* vol. 28, no. 2, pp. 335–343, Jun. 2013.
[15] Z. Wang, J. Ma, and L. Zhang, "Finite element thermal model and simulation for a cylindrical Li-ion battery," *IEEE Access* vol. 5, pp. 15372–15379, 2017.
[16] J. Jaguemont, L. Boulon, and Y. Dubé, "Characterization and modeling of a hybrid-electric-vehicle lithium-ion battery pack at low temperatures," *IEEE Trans. Veh. Technol.* vol. 65, no. 1, pp. 1–14, Jan. 2016.
[17] Y. Duan, J. Jiang, Z. Wang, F. Wen, and W. Shi, "Cooling simulation and experimental analysis on power lithium-ion battery pack," in *Proc. IEEE Conf. Expo Transp. Electrific. Asia–Pacific (ITEC Asia–Pacific)*, Aug./Sep. 2014, pp. 1–3.
[18] U. Seong, C. B. Shin, and C.-S. Kim, "Modeling for the scale-up of a lithium-ion polymer battery," *J. Power Sources* vol. 189, no. 1, pp. 841–846, 2009.
[19] U. Seong, "Modeling the thermal behaviors of a lithium-ion battery during constant-power discharge and charge operations," *J. Electrochem. Soc.*, vol. 160, no. 6, pp. A990–A995, 2016.
[20] D. Chen, "Modeling of a pouch lithium ion battery using a distributed parameter equivalent circuit for internal non-uniformity analysis," *Energies* vol. 9, no. 11, p. 865, 2016.
[21] M. Chen, "A multilayer electro-thermal model of pouch battery during normal discharge and internal short circuit process," *Appl. Therm. Eng.* vol. 120, pp. 506–516, Jun. 2017.
[22] D. Bernardi and E. Pawlikowski John Newman, "A general energy balance for battery systems," *J. Electrochem. Soc.* vol. 132, no. 1, pp. 5–12, 1985.
[23] S. Lin, "Battery modeling based on the coupling of electrical circuit and computational fluid dynamics," in *Proc. IEEE Energy Convers. Congr. Expo.*, Sep. 2011, pp. 2622–2627.
[24] J.-W. Kim and C.-S. Lee, "Co-simulation approach for analyzing electric-thermal interaction phenomena in lithium-ion battery," *Int. J. Precis. Eng. Manuf.-Green Technol.* vol. 2, no. 3, pp. 255–262, 2015.
[25] M. Einhorn, "Comparison, selection, and parameterization of electrical battery models for automotive applications," *IEEE Trans. Power Electron.*, vol. 28, no. 3, pp. 1429–1437, Mar. 2012.
[26] H. Rahimi-Eichi, F. Baronti, and M.-Y. Chow, "Online adaptive parameter identification and state-of-charge coestimation for lithium-polymer battery cells," *IEEE Trans. Ind. Electron.* vol. 61, no. 4, pp. 2053–2061, Apr. 2014.
[27] S. Liu, J. Jiang, W. Shi, Z. Ma, L. Y. Wang, and H. Guo, "Butler–volmer-equation-based electrical model for high-power lithium titanate batteries used in electric vehicles," *IEEE Trans. Ind. Electron.* vol. 62, no. 12, pp. 7557–7568, Dec. 2015.
[28] X. Hu, S. Li, and H. Peng, "A comparative study of equivalent circuit models for Li-ion batteries," *J. Power Sources* vol. 198, pp. 359–367, Jan. 20127.
[29] A. Seaman, T.-S. Dao, and J. McPhee, "A survey of mathematics-based equivalent-circuit and electrochemical battery models for hybrid and electric vehicle simulation," *J. Power Sources* vol. 256, pp. 410–423, Jun. 2014.
[30] J. Zhang, "Simultaneous estimation of thermal parameters for large-format laminated lithium-ion batteries," *J. Power Sources* vol. 259, pp. 106–116, Aug. 2014.
[31] S. Allu, "A new open computational framework for highly-resolved coupled three-dimensional multiphysics simulations of li-ion cells," *J. Power Sources* vol. 246, pp. 876–886, Jan. 2014.
[32] J. Zhang, "Comparison and validation of methods for estimating heat generation rate of large-format lithium-ion batteries," *J. Therm. Anal. Calorimetry* vol. 117, no. 1, pp. 447–461, 2014.
[33] X. Feng, "Influence of aging paths on the thermal runaway features of lithium-ion batteries in accelerating rate calorimetry tests," *Int. J. Electrochem. Sci.*, vol. 14, pp. 44–58, Jan. 2019.

WEINAN HUANG received the B.E. degree in electrical engineering from the China University of Petroleum, Qingdao, China, in 2017. He is currently pursuing the master's degree in electrical engineering with Beijing Jiaotong University. His research interests include the thermal simulation and management systems for the lithium ion battery.

WEIGE ZHANG received the M.S. and Ph.D. degrees in electrical engineering from Beijing Jiaotong University, Beijing, China, in 1997 and 2013, respectively, where he is currently a Professor with the School of Electrical Engineering. His research interests include battery pack application technology, power electronics, and intelligent distribution systems.

ANCI CHEN received the B.E. degree in electrical engineering from Beijing Jiaotong University, Beijing, China, in 2017, where he is currently pursuing the Ph.D. degree. His current research interest includes the thermal management systems for the lithium ion battery.

YANRU ZHANG received the B.E. and M.S. degrees in electrical engineering from Beijing Jiaotong University, Beijing, China, in 2012 and 2015, respectively. Her research interest includes the group application of the lithium-ion battery.

MING LI was born in 1983. He received the Ph.D. degree in aerodynamics. He is currently the Senior Engineer of CRRC Tangshan Company, Ltd., Tangshan, China. His main research interests include multidisciplinary optimization and aerodynamics.